Available online at www.sciencedirect.com
ScienceDirect
Ceramics International 34 (2008) 1241–1246
CERAMICS INTERNATIONAL
www.elsevier.com/locate/ceramint

Processing and microstructure characterization of porous corundum–spinel ceramics prepared by in situ decomposition pore-forming technique

Shujing Li *, Nan Li, Yawei Li

Hubei Province Key Laboratory of Refractories and Ceramics, 183#, Wuhan University of Science and Technology, Wuhan, Hubei 430081, PR China

Received 2 January 2007; received in revised form 20 February 2007; accepted 2 March 2007
Available online 19 April 2007

Abstract

Porous corundum–spinel ceramics were prepared from $Al(OH)_3$ and basic magnesium carbonate by an in situ decomposition pore-forming technique. Apparent porosity was detected by Archimedes' Principle with water as medium. Pore size distribution and the volume percentage of micropores were measured by mercury intrusion porosimetry, and the microstructure was analyzed by SEM. The apparent porosity of the sintered sample decreased with increasing the $Al(OH)_3$ content in the raw mixture. With increasing temperature from 1200 °C to 1300 °C the porosity of the sample increased rapidly, from 1300 °C to 1500 °C the apparent porosity increased slightly, while it decreased rapidly when the temperature increased from 1500 °C to 1600 °C. The pores in the samples consist of two groups. One group is composed of micropores whose diameter is mostly in the range from 150 nm to 300 nm while the other is composed of bigger pores whose diameter is in the range from 0.5 μm to 1 μm. It was found that the composition of the starting powders and the sintering temperature are responsible for the apparent porosity and the pore size distribution of the samples. However the spinel formation and sintering play a more important role on porosity and pore size distribution.

Keywords: In situ decomposition; Pore-forming; Porous; Corundum–spinel

1. Introduction

Recently, there has been an increasing interest in the applications of porous ceramics as filters, desiccants, insulators, catalyst supports, bone replacement, acoustic absorbers, sensors and membrane reactors [1–6].

Porous ceramics can be made by adding pore-forming agents such as sawdust, starch, graphite or organic particulates [7] into the starting powers, or by injection molding [8], or by gelcasting [1]. Deng et al. made porous alumina ceramics by the decomposition of $Al(OH)_3$ [9,10]. This in situ decomposition pore-forming technique exploiting the decomposition of starting powders is a good way to prepare porous ceramics containing well-distributed pores. The present authors also studied the preparation of porous corundum–mullite ceramics using $Al(OH)_3$ powder and silica micro powder [11] and using $Al(OH)_3$ and kaolinite gangue [12].

Spinel ($MgAl_2O_4$) possesses a unique combination of desirable properties: high melting point (2135 °C), high resistance against chemical attack, good mechanical strength both at room temperature and elevated temperatures. It has a lower thermal-expansion coefficient and better thermal shock resistance than MgO and Al_2O_3 [13–15]. Despite the fact that most of the studies were conducted on stoichiometric spinel [16–18], it is well known that spinel shows a wide range of non-stoichiometry between alumina and magnesia [19,20]. If it is considered the smaller elastic modulus and thermal expansion coefficient, porous corundum–spinel ceramics should have better thermal shock resistance than corundum and magnesia porous ceramics. This article describes some results of the microstructure characterization and final physical properties of corundum–spinel porous ceramics prepared by in situ decomposition pore-forming technique.

* Corresponding author. Tel.: +86 27 68862188; fax: +86 27 68862018.
E-mail addresses: lsjrose@21cn.com (S. Li), linanref@public.wh.hb.cn (N. Li), liyaweiref@hotmail.com (Y. Li).

0272-8842/$34.00
doi:10.1016/j.ceramint.2007.03.018

Table 1
Chemical compositions of raw material (wt%)

	SiO_2	Al_2O_3	Fe_2O_3	CaO	MgO	K_2O	Na_2O	IL
$4MgCO_3{\cdot}Mg(OH)_2{\cdot}5H_2O$	0.05	0.19	0.02	0.04	42.69	–	–	57.06
$Al(OH)_3$	0.002	66.85	0.041	0.15	0.04	0.013	0.039	32.60

2. Experimental procedure

The starting materials used in this study are $Al(OH)_3$ and an analytical reagent grade of basic magnesium carbonate ($4MgCO_3{\cdot}Mg(OH)_2{\cdot}5H_2O$). Chemical compositions of the raw material are listed in Table 1. In order to get fine powders with uniform particle size, $Al(OH)_3$ and basic magnesium carbonate powders were sieved and picked between 200 mesh and 270 mesh. The preparations of $Al(OH)_3$ and basic magnesium carbonate on the different compositions are shown in Table 2. These three types of starting powders were wet mixed for 1 h in ethanol and pressed at 50 MPa in a stainless steel die to make the billets with a diameter of 20 mm and a height of 20 mm. The green compacts were dried at 110 °C for 24 h, and then sintered at 1200 °C, 1300 °C, 1400 °C, 1500 °C and 1600 °C for 3 h, respectively.

Apparent porosity was detected by Archimedes' Principle with water as medium. Linear changes were obtained by comparing the diameter of the specimens before and after sintering. The pore size distribution was measured by mercury intrusion porosimetry (AutoPore IV 9500, Micromeritics Instrument Corporation) and the microstructure was analyzed by SEM (Philips XL 30 TMP scanning electron microscope). True density was measured by a helium pycnometer (Micromeritics, ACCUPYC 1330). X-ray diffraction (Philips X'pert TMP) was used to analyze phase compositions in the specimens sintered at different temperatures. In addition, the relative content of $MgAl_2O_4$ in the sintered specimens was evaluated using the standard-free quantitative method [21]. This is not an accurate method to evaluate phase content in samples, but it can be used to compare the phase content in samples processed under the same conditions. The phase content can be calculated from the following formula:

$$\sum_{i=1}^{n}\left[\left(1-\frac{I_{iJ}}{I_{iK}}\right)x_{iK}\mu_{mi}\right]=0, \qquad \sum_{i=1}^{n}x_{iK}=1 \tag{1}$$

where I_{iJ} and I_{iK} are, respectively, the intensities of i phase in samples J and K, respectively, x_{iK} the content of i phase in sample K and μ_{mi} is the mass absorption coefficient in i phase.

Table 2
Main compositions of different starting powders (wt%)

	1#	2#	3#
$Al(OH)_3$	65	80	90
$4MgCO_3{\cdot}Mg(OH)_2{\cdot}5H_2O$	35	20	10
Spinel[a]	100	50	24

[a] The content of spinel in the sintered specimens calculated from the starting powders.

3. Results and discussion

3.1. The effect of the ratio between $Al(OH)_3$ and $MgCO_3$ in the starting powders, on the pore size distribution of the sintered specimens

The effect of the $Al(OH)_3$ content in the starting powders over the apparent porosities and the linear changes are shown in Fig. 1. It can be noticed in Fig. 1 that as the $Al(OH)_3$ content increases, both the apparent porosities and the linear changes of the sintered specimens decrease. The pore size distributions of the specimens prepared from different starting powders sintered at 1500 °C are shown in Fig. 2. They are visibly bimodal in distribution. One group is composed of micropores whose diameter is mostly in the

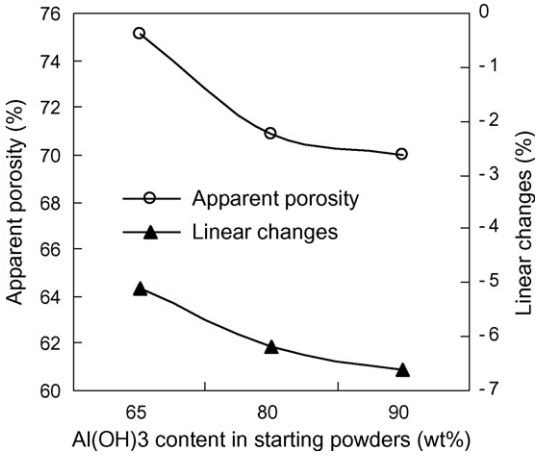

Fig. 1. Variations of the apparent porosities and the linear changes of the specimens sintered at 1500 °C for 3 h with the composition of the starting powders.

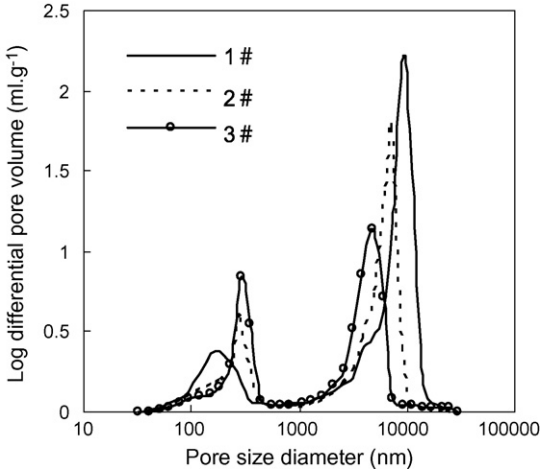

Fig. 2. Variation of the pore size distribution of the porous specimens with different starting powders sintered at 1500 °C for 3 h.

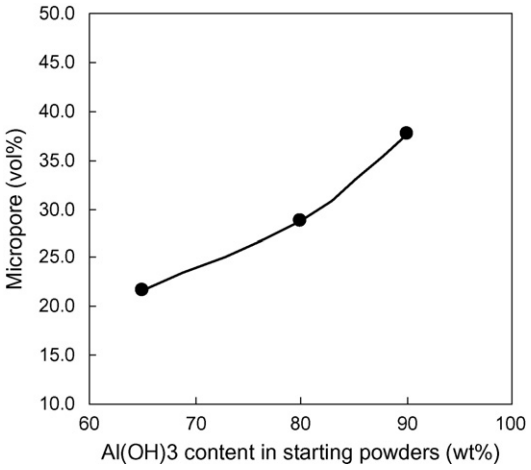

Fig. 3. Variation in the micropore vol% with different starting powders sintered at 1500 °C for 3 h.

range from 150 nm to 300 nm, while the other group is composed of bigger pores whose diameter is in the range from 0.5 μm to 1 μm. With increasing the $Al(OH)_3$ content in the starting powders the pore size diameter of the micropores increase. However, the size of bigger pores decreases.

In Fig. 3 it is presented the volume percentage of micropores (pore size ≤400 nm) of the total pore volume (micropore vol%). It was found that with increasing the $Al(OH)_3$ content in the starting powders the micropore vol% of the sintered specimen increased. Based on the results presented previously, we may conclude that sample No. 2 displays the best characters because it has higher porosity (up to 70.8%) and a higher concentration of micropores (up to 28.3 vol%).

3.2. The effect of sintering temperature on the apparent porosity and the pore size distribution of the specimen

In Fig. 4 it is shown the apparent porosities of the specimen No. 2 sintered at different temperatures. The pore size distributions of the sample No. 2 sintered at different temperatures are illustrated in Fig. 5. The micropore vol% as a function of the sintering temperature is shown in Fig. 6. From an analysis of the sets presented in the three figures it can be concluded that the curves can be divided into three temperature ranges. From 1200 °C to 1300 °C, the apparent porosity of the sintered samples increases rapidly, while the micropore size changes a little. On the other hand the ratio of micropore volume to total pore volume decreases and the size of bigger pores increases considerably. From 1300 °C to 1500 °C, the apparent porosity increases and the micropore vol% decreases slightly, but the size of micropores and bigger pores increase considerably. From 1500 °C to 1600 °C, the apparent porosity decreases abruptly, micropore size increases, and bigger pore size and micropore vol% decrease considerably.

3.3. Discussion

The resulting microstructure of the porous corundum–spinel composites of this study, prepared by in situ decomposi-

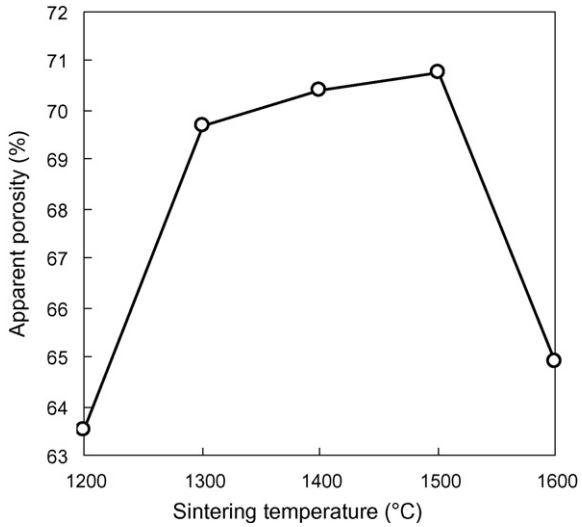

Fig. 4. Dependence of the apparent porosity of the sintered specimen No. 2 on the sintering temperature.

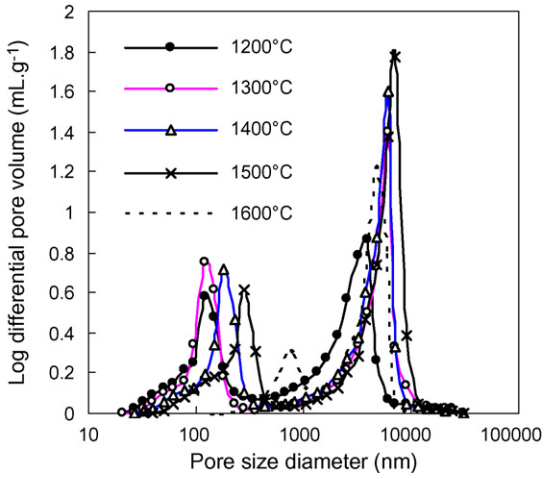

Fig. 5. Variation in the pore size distribution with the sintering temperature for the specimen prepared from the powders No. 2.

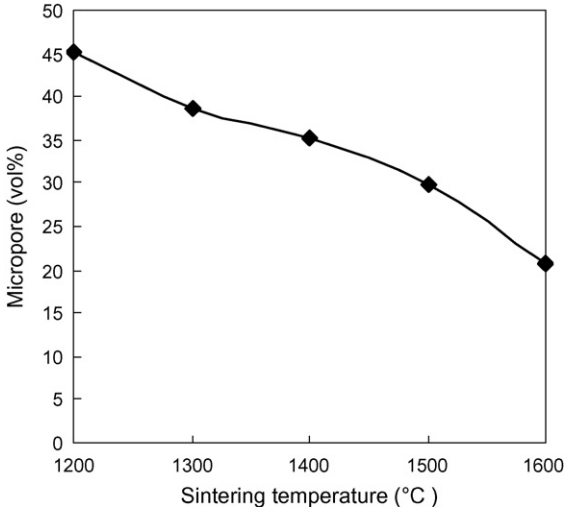

Fig. 6. Variation in the micropore vol% with the sintering temperature for the specimen No. 2.

Table 3
True density of minerals concerned (g/cm^3)

Corundum, Al_2O_3	3.93
Periclase, MgO	3.47
Spinel, $MgAl_2O_4$	3.60
Basic magnesium carbonate, $4MgCO_3{\cdot}Mg(OH)_2{\cdot}5H_2O$	2.15
Gibbsite, $Al(OH)_3$	2.49

tion pore forming technique, depends on the following parameters:

1. The expansion caused by the formation of the spinel phase.
2. The degree of packing in the green body.
3. The difference in true density of the starting materials.
4. The difference in true density between the phases formed during sintering.

In Table 3 it is shown the true density of all the phases involved. The difference in true density between corundum and gibbsite is the largest among the used components. It should be expected that the more the gibbsite content in the green compacts, the higher the pore volume produced in the sintered samples. However the increase of $Al(OH)_3$ content in the starting powders leads to a decrease in the porosity of the sintered samples. This means that the difference between true density of the minerals in the sintered samples and the true density of minerals in the green samples is not the determining factor on the porosity of sintered samples. The decomposition of $Al(OH)_3$ and basic magnesium carbonate creates pores in the early stage of firing. However, the pore volume action and size distribution are controlled by spinel formation and sintering at the end of the firing process. With increasing of $Al(OH)_3$ content, the expansion resulting from the spinel formation decreases, while the formation of Al_2O_3 crystallites which have high sinterability increases. As a result, by increasing the $Al(OH)_3$ content in the starting powders, the porosity of sintered samples decreases and the linear shrinkage increases (Fig. 1).

It can be seen that the grains in the samples sintered at 1500 °C keep the contour of the original $Al(OH)_3$ or basic magnesium carbonate grains, these are called ''pseudomorphs''. This phenomenon was also found in the sintering of MgO made from magnesite [22,23]. Li [22] proposed that that ''pseudomorphs'' were composed of aggregates of crystallites and the compact which was found by the aggregates had actually a multiple-particle packing strcture. The aggregate particles consist of crystallites of Al_2O_3 and spinel ($MgO{\cdot}Al_2O_3$) as shown in Fig. 7. The crystallites inside the pseudomorphs are called ''primary particles''. The micropores having diameter $\leq$400 nm, with maximum diameter between 150 nm and 300 nm, which are formed by the decompositions of $Al(OH)_3$ and basic magnesium carbonate, are located among the primary particles. They are called ''primary pores''; the pseudomorph grains are called ''secondary particles''. The bigger pores having diameter >1 μm which are located among the secondary particles are called ''secondary pores''.

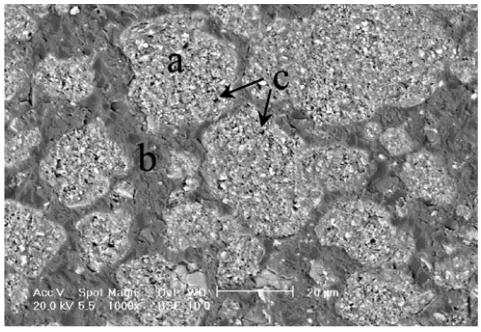

Fig. 7. SEM image of a polished surface of the specimen No. 2 sintered at 1500 °C for 3 h. (a) Secondary particle, (b) secondary pore and (c) Primary pore.

The expansion resulting from the spinel formation and the shrinkage resulting from the sintering of Al_2O_3 and spinel crystallites, affect the porosity and the size distribution of primary and secondary pores. The expansion resulting from spinel formation fills the primary pores in the pseudomorphs and decreases the size and volume fraction of primary pores. On the other hand the shrinkage resulted from sintering of crystallites, mainly Al_2O_3 crystallites in pseudomorphs, leads to increasing of the size and volume of the primary pores. In samples from Nos. 1 to 3, the spinel content in the sintered samples decreased, while the Al_2O_3 crystallite size increased. This resulted in the increase of primary pore size (Fig. 2) and volume (Fig. 3). The curve related to the primary pores size distribution in sample No. 1 is rather broad. It indicates that some very small pores have been filled up.

On the other hand the pseudomorphs size also changes during sintering. Usually, pseudomorphs will shrink in the early time of sintering because of the decomposition of basic magnesium carbonate and $Al(OH)_3$ and the sintering of MgO and Al_2O_3 inside the pseudomorphs. The shrinkage resulted from the rearrangement of pseudomorph grains in the samples early in the sintering process leads to the decrease in the secondary pore size and volume [22]. With the increase of $Al(OH)_3$ content in the starting powders (from Nos. 1 to 3), the resulting spinel content in the sintered samples decreases. On the other hand the shrinkage of pseudomorphs increases. This results in a stronger rearrangement of the pseudomorphs in the samples. This is responsible for the decrease in the secondary pore size and volume (Fig. 2).

In Fig. 8 it is shown the XRD patterns of sample No. 2 heated at different temperatures. Upon raising the sintering temperature, the content of spinel in the sintered samples increases. In Fig. 9 it is shown the relative contents of spinel in the samples heated at different temperatures. The curve of Fig. 9 can also be divided into three parts as presented in Figs. 4 and 6. It can be seen that the spinel content from 1200 °C to 1300 °C in the sintered samples increases with temperature resulting an increased expansion. At the same time the sintering occurs slowly because of the low sintering temperature, leading to an abrupt increase in the apparent porosity (Fig. 4) as well as a decrease in the micropore vol% (Fig. 6). From 1300 °C to 1500 °C the rate of spinel formation and sintering occurs faster

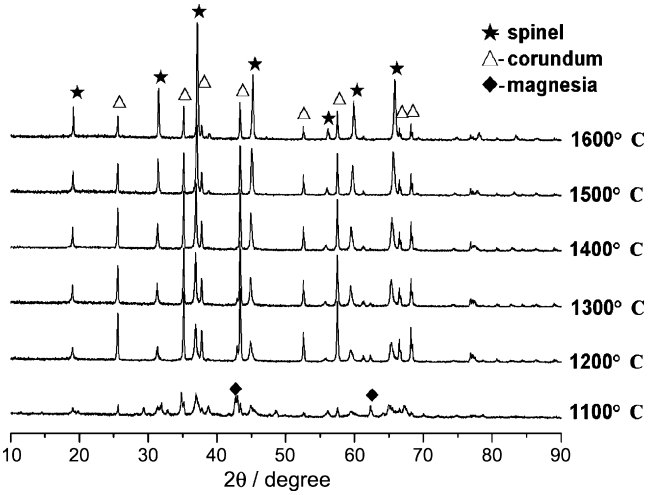

Fig. 8. The XRD analyses of the specimen No. 2 sintered at different temperatures.

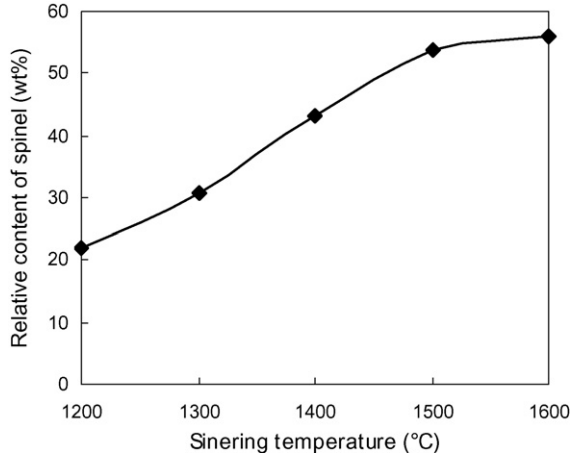

Fig. 9. Relative content of spinel in the sample No. 2 sintered at different temperatures.

than those from 1200 °C to 1300 °C. The sintering of Al_2O_3 crystallites with high activity in the pseudomorphs takes place very fast. The shrinkage resulting from the sintering overrides the expansion resulting from spinel formation, and lead to the growth of primary pores (Fig. 5). At the same time, in this period of sintering, the rearrangement of the pseudomorphs cannot take place because connections among pseudomorphs are formed. The shrinkage of pseudomorphs results in the growth of secondary pores (Fig. 5). In the temperature raises from 1500 °C to 1600 °C, a large amount of spinel is produced. In this stage the rate of spinel formation becomes very slow, but the sintering occurs very fast because of the higher temperature level. This results in the increase of primary pores size, while the size and volume of secondary pores decrease. In addition the apparent porosity decreases rapidly.

4. Conclusions

The in situ decomposition pore-forming technique has been successfully employed to fabricate porous corundum–spinel ceramics using $Al(OH)_3$ and basic magnesium carbonate as presents. It was found that the compositions of the starting powders and the sintering temperature are responsible for the apparent porosity and the pore size distribution of the sintered samples. The apparent porosity of the sintered sample decreases with the increase of $Al(OH)_3$ content in the raw mixture. By increasing temperature from 1200 °C to 1300 °C the porosity of the samples increases rapidly. From 1300 °C to 1500 °C the apparent porosity increases slightly, while it decreases rapidly when the temperature is increased from 1500 °C to 1600 °C. The pores in the samples consist of two groups. One group is related to micropores whose diameter is mostly in the range from 150 nm to 300 nm. The other group is composed of bigger pores whose diameter is in the range from 0.5 μm to 1 μm. It was also found that the composition of the starting powders and the sintering temperature are responsible for the apparent porosity and the pore size distribution of the samples. However the spinel formation and its sintering play a more important role on porosity and pore size distribution.

References

[1] Y.F. Liu, X.Q. Liu, H. Wei, G.-Y. Meng, Porous mullite ceramics from national clay produced by gelcasting, Ceram. Int. 27 (2001) 1–7.
[2] Z.R. Ismagilov, R.A. Shkrabina, N.A. Koryabkina, et al., Porous alumina as a support for catalysts and membranes. Preparation and study, React. Kinet. Catal. Lett. 60 (2) (1997) 225–231.
[3] S. Kwon, et al., Constrained densification in boehmite–alumina mixtures for the fabrication of porous alumina ceramics, J. Mater. Sci. 33 (1998) 913–921.
[4] Y.M. Jo, Characterization of ceramic composite membrane filters for hot gas cleaning, Power Technol. 91 (1) (1997) 55–62.
[5] M. Bennasar, D. Rouleau, R. Mayer, et al., Ultrafiltration of milk on mineral membranes: improve performance, J. Soc. Dairy Technol. 35 (2) (1982) 43–49.
[6] J. Coronas, M. Menendez, J. Santamaria, Methane oxidative coupling using porous ceramic membrane reactors, Chem. Eng. Sci. 49 (12) (1994) 2005–2013.
[7] J.H. She, T. Ohji, Fabrication and characterization of highly porous mullite ceramics, Mater. Chem. Phys. 80 (2003) 610–614.
[8] X. Zhipeng, et al., Study on binder removal process of ceramics injection molding, J. Chinese Ceram. Bull. 2 (1998) 18–21.
[9] Z.-Y. Deng, T. Fukasawa, M. Ando, Microstructure and mechanical properties of porous alumina ceramics fabricated by the decomposition of aluminum hydroxide, J. Am. Ceram. Soc. 84 (11) (2001) 2638–2644.
[10] Z.-Y. Deng, T. Fukasawa, M. Ando, High-surface-area alumina ceramics fabricated by the decomposition of $Al(OH)_3$, J. Am. Ceram. Soc. 84 (3) (2001) 485–491.
[11] S. Li, N. Li, Influence of composition of starting powders and sintering temperature on the pore size distribution of porous corundum–mullite ceramics, Sci. Sinter. 37 (3) (2005) 173–180.
[12] S. Li, N. Li, Effects of composition and temperature on porosity and pore size distribution of porous ceramics prepared from $Al(OH)_3$ and kaolinite gangue, Ceram. Int. 33 (4) (2007) 551–556.
[13] M. Sindel, N.A. Travitzky, et al., Influence of magnesium–aluminum spinel on the directed oxidation of molten aluminum alloys, J. Am. Ceram. Soc. 73 (9) (1990) 2615–2618.
[14] G. Baudin, R. Martinez, et al., High-temperature mechanical behavior of stoichiometric magnesium spinel, J. Am. Ceram. Soc. 78 (7) (1995) 1857–1862.
[15] J.-G. Li, T. Ikegami, et al., A wet-chemical process yielding reactive magnesium aluminate spinel ($MgAl_2O_4$) powder, Ceram. Int. 27 (2001) 481–489.
[16] A. Granon, P. Goeuriot, et al., Aluminum magnesium oxynitride: a new transparent spinel ceramic, J. Eur. Ceram. Soc. 15 (1995) 249–254.

[17] T.A. Bazilevskaya, V.T. Gritsyna, et al., The effect of composition, processing conditions, and irradiation, on lattice defects in spinel ceramics, J. Nucl. Mater. 253 (1998) 133–140.
[18] R.A. Candeia, M.I.B. Bernardi, et al., Synthesis and characterization of spinel pigment $CaFe_2O_4$ obtained by the polymeric precursor method, Mater. Lett. 58 (2004) 569–572.
[19] T. Yano, A. Insani, et al., Neutron-induced damage in near-stoichiometric spinel ceramics irradiated below 200 °C and its recovery due to annealing, J. Nucl. Mater. 258–263 (1998) 1836–1841.
[20] T. Yano, H. Sawada, et al., Recovery of neutron-induced defects in near-stoichiometric spinel ceramics irradiated at around 500 °C, Nucl. Instrum. Meth. Phys. Res. B 116 (1996) 131–135.
[21] C. Ynag, D. Xie, et al., Phase Diffraction Analysis, Metallurgical Industry Publishing House, 1989,, p. 158.
[22] N. Li, Sintering mechanism and models of aggregated MgO powder compacts, Sci. Sinter. 24 (3) (1992) 161–171.
[23] N. Li, Formation, compressibility and sintering of aggregated MgO powder, J. Mater. Sci. 24 (1989) 485–492.